Hinge Angles for 3D Discrete Rotations*

Yohan Thibault[1], Akihiro Sugimoto[2], and Yukiko Kenmochi[1]

[1] Université Paris-Est, LIGM, UMR UPEMLV/ESIEE/CNRS 8049, France
{thibauly,y.kenmochi}@esiee.fr
[2] National Institute of Informatics, Japan
sugimoto@nii.ac.jp

Abstract. In this paper, we focus on 3D rotations on grid points computed by using only integers. For that purpose, we study the intersection between the 3D half-grid and the rotation plane. From this intersection, we define 3D hinge angles which determine a transit of a grid point from a voxel to its adjacent voxel during the rotation. Then, we give a method to sort all 3D hinge angles with integer computations. The study of 3D hinge angles allows us to design a 3D discrete rotation.

Keywords: discrete geometry, discrete rotation, half-grid, multi-grid, hinge angle, integer computation.

1 Introduction

Rotations in the 3D space are required in many applications for computer imagery, such as image processing [13], computer vision [7,10] and computer graphics [6]. A rotation in the 3D Euclidean space can be in general represented in two different typical ways. One is to represent a rotation as a combination of three particular rotations around the three axes of the coordinate system in concern [14]. The other is to represent a rotation by a rotation axis together with an angle around the axis [7,10]. Even if the representations of a rotation are different, computed rotation results are the same as far as the space is continuous. However, this is not the case for the discrete space. Namely, depending on the rotation representation, the computed rotation result can change in the discrete space [2]. As is the case of 2D rotations, computing a 3D rotation once in the discrete space brings displacement from that in the continuous space; computing 3D rotations many times causes difficulty in analyzing inherited displacements during the computation. Accordingly, representing a 3D rotation by a rotation axis together with an angle around the axis is more preferable in the 3D discrete space. Besides, it is known that such axis-angle representation is useful for 3D rotation estimation from given image sets, which is one of important problems in computer vision [7,10].

In [8], the author proved that a 2D discrete image have a finite number of different rotation. This number is directly related to the number of hinge angles.

The extension of hinge angles for the 3D space allows to obtain the same result. This result can be useful for some problems such as the pose problem. In order to obtain the optimal solution, the pose problem need to try all different rotation, which is impossible in continuous space since there exists an infinity of rotation [7]. Using hinge angles for this problem can help to reach the optimal solution.

This paper presents a study of the rotation in the 3D discrete space. Since we admit only integer computations, we assume that our rotation center is a grid point such as the origin, and that a rotation axis has integer coordinates. In the 2D case, hinge angles are known to correspond to the discontinuity caused by discretisation of the rotation in the continuous plane [1,8,12]. Intuitively, hinge angles determine a transit of a grid point from a pixel to its adjacent pixel during the rotation. In other words, two rotations with nearby angles transform the same grid point to two adjacent pixels because discrete rotations around a given center are locally continuous with regard to the angle. Hinge angles are their discontinuity angles. Computing hinge angles using integers alone allows us to compute 2D discrete rotations without any approximation errors, which designs the 2D discrete rotation. Extending these to the 3D case, we design a 3D discrete rotation. In the 3D case, however, depending on the rotational axis, we have a variety of transitions of a grid point across voxels. How to capture these transitions systematically is a big issue.

We define hinge angles for 3D rotations so that they determine a transit of a grid point from a voxel to its adjacent voxel. To compute the hinge angles using integers alone, we pay our attentions to the intersection of voxels and a given rotation plane to define convexels. The variety of transitions of a grid point across voxels in 3D results in the variation of convexels in 2D. We then compute the hinge angles by using the intersection between the convexel and a locus of the rotation in the rotation plane. Finally, we give a method to sort all the possible hinge angles in concern to design a 3D discrete rotation. Differently from 2D discrete rotations [2,8,3], few attempts on 3D discrete rotations have been reported [13,6]. In particular, to our best knowledge, this is the first work on 3D discrete rotation using integer computation without digitization errors.

2   Hinge Angles

Hinge angles for 2D rotations are defined to represent the discontinuities of rotations in the discrete plane [8]. Hinge angles determine a transit of a grid point from a pixel to its adjacent pixel during the rotation. To characterize those hinge angles, the 2D half-grid plays an important role.

Definition 1. *The half-grid in the plane is the set of lines, each of which is represented by one of $x = i + \frac{1}{2}$ and $y = i + \frac{1}{2}$ where $i \in \mathbb{Z}$.*

In other words, the 2D half-grid represents the border between two adjacent pixels. From the definition of the 2D half-grid, we define the hinge angles in the plane.
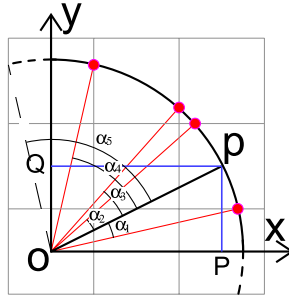
Fig. 1. All hinge angles in the first quadrant for the grid point $\boldsymbol{p} = (2, 1)^\top$, such that $\alpha_1 \approx -13.68°$, $\alpha_2 \approx 15.59°$, $\alpha_3 \approx 21.31°$, $\alpha_4 \approx 50.52°$, $\alpha_5 = \frac{\pi}{2} - \alpha_1 \approx 76.32°$

Definition 2. *An angle α is called a hinge angle if at least one point in $\mathbb{Z}^2$ exists such that its image by the Euclidean rotation with α around the origin is on the 3D half-grid.*

Figure 1 illustrates some examples of hinge angles for the grid point $(2, 1)^\top$. It presents all the hinge angles in the first quadrant. Note that hinge angles in other quadrants are obtained by symmetry with respect to the x-axis and/or y-axis from those in Figure 1.

To extend the definition of hinge angles into the 3D case, we first define the half-grid in the 3D space. Similarly to the 2D half-grid, the 3D half-grid defines the limit between two adjacent voxels in the 3D discrete space.

Definition 3. *The half-grid in the 3D space is the set of planes, each of which is represented by one of $x = i + \frac{1}{2}, y = i + \frac{1}{2}$ and $z = i + \frac{1}{2}$ where $i \in \mathbb{Z}$.*

Introducing the definition of the half-grid in the 3D space allows us to define hinge angles in 3D as a natural extension of hinge angles in 2D. As mentioned in the introduction, we only consider here 3D rotations whose rotation axes have integer coordinates and go through the origin. Hereafter, we call such an axis an integer-axis.

Definition 4. *An angle α is called a hinge angle if at least one point in $\mathbb{Z}^3$ exists such that its image by the Euclidean rotation with α around an integer-axis is on the half-grid.*

Similarly to the case of 2D, for a grid point $\boldsymbol{p}$ in 3D, an angle α is a hinge angle if and only if the discretised point of the rotation result of $\boldsymbol{p}$ with angle $\alpha + \epsilon$ becomes different from that with angle $\alpha - \epsilon$ for any $\epsilon > 0$.

Differently from the case of 2D rotations, we need not only a rotation angle but also a rotation axis in order to specify a 3D rotation. This requires investigation of the intersection between voxels and a plane determined by a given rotation axis because a variety of transitions of a grid point across voxels exist depending on the plane. To capture this variety, we introduce the multi-grid in the next section, which allows us to compute hinge angles in the 3D rotation plane.

(a)   (b)
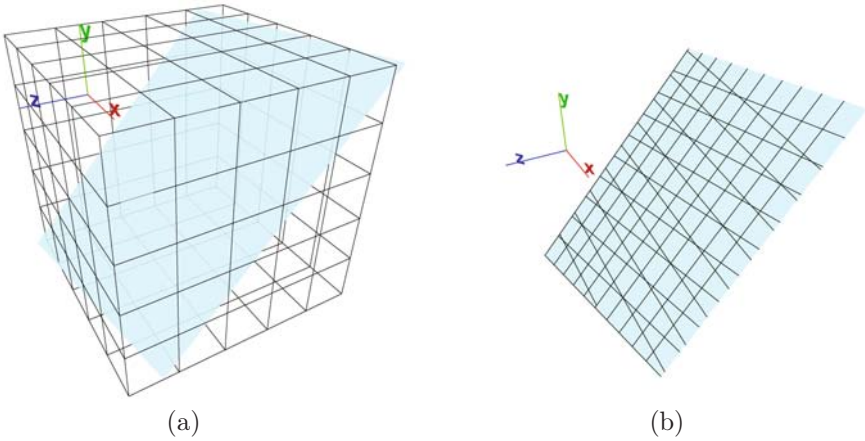
Fig. 2. The 3D half-grid cut by a plane (a), and its multi-grid (b)

3 Hinge Angles in a Rotation Plane

A 3D rotation is represented by a rotation axis and a rotation angle. Accordingly, the 3D rotation of a given grid point is considered as the 2D rotation of the point in the rotation plane that is defined as the plane going through the grid point and having the normal vector parallel with the rotation axis. In this section, we capture hinge angles in a given rotation plane.
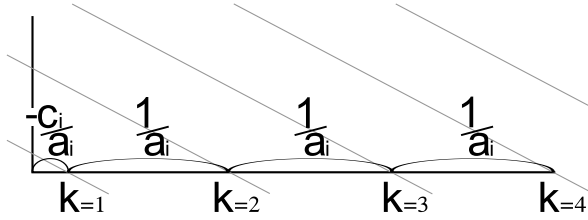
3.1 Multi-grid

When a rotation plane in 3D is given, we consider the intersection between the plane and the half-grid in the 3D space as illustrated in Figure 2(a). As we see, the intersection consists of three different sets of parallel lines as illustrated in Figure 2(b), except for cases where the normal of the rotation plane is parallel to one of the axes defining the coordinate system of the 3D space. As such exceptional cases provide only two different sets of parallel lines, which are identical with those of the 2D half-grid, we here do not take into account those cases. In other words, in such cases, 3D rotations become identical with 2D rotations. We call the three different sets of parallel lines a multi-grid, which is used for characterizing hinge angles for 3D rotations instead of the 2D half-grid for 2D rotations.

In a multi-grid, the interval between parallel lines having the same directional vector is regular. Normalizing the interval allows us to represent a set of parallel lines having the same directional vector as

$$\{(x,y)^\top \in \mathbb{R}^2 | ax + by + c + k = 0, a^2 + b^2 \neq 0, k \in \mathbb{Z}, a, b, c \in \mathbb{R}\}. \quad (1)$$

The integer parameter k denotes the index number of each parallel line. Figure 3 gives a geometrical explanation of the parameters of a set of parallel lines. For

Fig. 3. Parallel lines of a set $\mathcal{M}_i^{\mathcal{A},\boldsymbol{p}}$ and geometric interpretation of their parameters

example, if a point $(x, y)^\top$ is on one of the parallel lines, $(x - \frac{k}{a}, y)^\top$ is on the k-th next line, providing that $a \neq 0$. Now we can give a formal definition of a multi-grid.

Definition 5. *Let* $\mathcal{M}_i = \{(x, y)^\top \in \mathbb{R}^2 | a_i x + b_i y + c_i + k = 0, a_i^2 + b_i^2 \neq 0, k \in \mathbb{Z}, a_i, b_i, c_i \in \mathbb{R}\}$ *for* $i = 1, 2, 3$ *be each set of parallel lines induced from a given rotation plane and the 3D half-grid. Then the multi-grid* $\mathcal{M}$ *is the union of* $\mathcal{M}_i$: $\mathcal{M} = \cup_i \mathcal{M}_i$.

The multi-grid in the rotation plane forms various convex polygons surrounded by lines, which we call convexels. Depending on the rotation plane, we have a variety of shapes of convexels. The shapes of convexels are investigated in [4] under the context of the intersection of a voxel and a plane, and the number of vertices of a convexel can be 3, 4, 5 or 6 as illustrated in Figure 4. The convexel is the counterpart of the squared pixel defined in the 2D plane. We remark that when the normal of the rotation plane is parallel with one of the axes defining the coordinate system of the 3D space, the notion of convexels coincides with the notion of pixels.

The following proposition allows us to characterize hinge angles in the framework of multi-grids, instead of the half-grid.

Proposition 1. *Let* $\boldsymbol{p}$ *be a grid point and* $\boldsymbol{p}'$ *be the result of the rotation of* $\boldsymbol{p}$ *by an angle* α *around an integer-axis. If* α *is a hinge angle, then* $\boldsymbol{p}'$ *is on the multi-grid.*
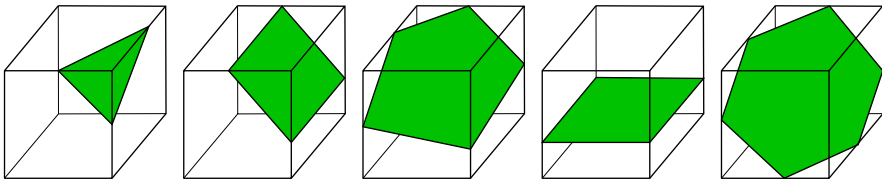
Fig. 4. The five different shapes of convexels, which are constructed as the intersections between a rotation plane and voxels [4]

3.2 Hinge Angles and Multi-grids

In 2D, there exists a property on hinge angles ensuring that the locus of rotation of a grid point cannot contain the intersection of two lines belonging to the half-grid [8]. In this section, we show that the same property for the hinge angles in the rotation plane holds. Namely, we show that, for a given multi-grid, the locus of the rotation of a grid point does not go through any vertex of convexels in the multi-grid.

Hereafter, we denote by $\mathcal{M}^{\mathcal{A},\boldsymbol{p}}$ the multi-grid defined by a rotation plane with a normal vector $\mathcal{A} = (a_x, a_y, a_z)^\top$ going through point $\boldsymbol{p} = (p_x, p_y, p_z)^\top$ and by $\boldsymbol{A}$ the axis of rotation of directional vector $\mathcal{A}$ going through the origin.

Proposition 2. *Let $\mathcal{M}^{\mathcal{A},\boldsymbol{p}}$ be a multi-grid where $\mathcal{A} \in \mathbb{Z}^3$ and $\boldsymbol{p} \in \mathbb{Z}^3$. Then, the locus of the rotation of $\boldsymbol{p}$ around $\boldsymbol{A}$ does not go through any vertex of the convexels on $\mathcal{M}^{\mathcal{A},\boldsymbol{p}}$.*

Proof. *The equation of the rotation plane $\mathcal{P}$ of $\mathcal{M}^{\mathcal{A},\boldsymbol{p}}$ is $a_x x + a_y y + a_z z - \mathcal{A}.\boldsymbol{p} = 0$. Let $\boldsymbol{p}' = (p'_x, p'_y, p'_z)^\top$ be a point which belongs to the locus of the rotation of $\boldsymbol{p}$ in $\mathcal{P}$ around $\boldsymbol{A}$. Let us assume that $\boldsymbol{p}'$ is also a vertex of a convexel of $\mathcal{M}^{\mathcal{A},\boldsymbol{p}}$, so that it belongs to two planes of the 3D half-grid. Thus we can set, without loss of generality, that $p'_x = k_x + \frac{1}{2}$ and $p'_y = k_y + \frac{1}{2}$ where $k_x, k_y \in \mathbb{Z}$, and then $\boldsymbol{p}' = (k_x + \frac{1}{2}, k_y + \frac{1}{2}, p'_z)^\top$.*

The locus of the rotation of $\boldsymbol{p}$ is the intersection between $\mathcal{P}$ and the sphere $\mathcal{S}$: $x^2 + y^2 + z^2 - (p_x^2 + p_y^2 + p_z^2) = 0$. Thus, by the assumption that $\boldsymbol{p}'$ belongs to $\mathcal{P}$ and $\mathcal{S}$, we have

$$a_x \left(k_x + \frac{1}{2} \right) + a_y \left(k_y + \frac{1}{2} \right) + a_z p'_z - \mathcal{A}.\boldsymbol{p} = 0, \tag{2}$$

$$\left(k_x + \frac{1}{2} \right)^2 + \left(k_y + \frac{1}{2} \right)^2 + p'^2_z - (p_x^2 + p_y^2 + p_z^2) = 0. \tag{3}$$

From (2) we see that p'_z must be a rational number, so that there exists a pair of integers λ_1, λ_2 such that $p'_z = \frac{\lambda_1}{\lambda_2}$ and $\gcd(\lambda_1, \lambda_2) = 1$. From (3) we see that $p'^2_z + \frac{1}{2}$ must be an integer. Thus we have

$$p'^2_z = \frac{\lambda_1^2}{\lambda_2^2} = k + \frac{1}{2}, \tag{4}$$

where $k, \lambda_1, \lambda_2 \in \mathbb{Z}$. Since $\gcd(\lambda_1, \lambda_2) = 1$ and $2\lambda_1^2 = (2k + 1)\lambda_2^2$, λ_2 must be even. Setting $\lambda_2 = 2\lambda'_2$ where $\lambda'_2 \in \mathbb{Z}$, we then obtain $2\lambda_1^2 = 4(2k + 1)\lambda'^2_2$ and deduce that λ_1 must be also even, which contradicts the assumption that $\gcd(\lambda_1, \lambda_2) = 1$.

Therefore we can conclude that there is not such a point $\boldsymbol{p}'$.   □

This proposition shows that two adjacent convexels, where the transition of $\boldsymbol{p}$ during its rotation is done between them, always share a convexel edge. In other words, the circle of $\boldsymbol{p}$ around $\boldsymbol{A}$ passes through a sequence of voxels such that any successive voxels are connected by their common face.

4   Integer Representation of Hinge Angles

The goal of this section is to show how to obtain the unique representation of an integer quintuplet for a 3D hinge angle, namely an injective map from hinge angles to quintuplets. We first explain how to obtain the equations representing lines in a multi-grid provided that the rotation plane is given. Then, we represent 3D hinge angles using five integers and then explain how to decode them to obtain the hinge angle. Note that the rotation plane is defined by a normal vector A and a point p on the plane, and we assume in the following that $\mathcal{A}$ and $\boldsymbol{p}$ are given. Thus a multi-grid is denoted by $\mathcal{M}^{\mathcal{A},\boldsymbol{p}} = \cup_{i=1,2,3}\mathcal{M}_i^{\mathcal{A},\boldsymbol{p}}$.

4.1   Multi-grid Line Equations

In Section 3, we explained that we do not consider the cases where the vector $\mathcal{A}$ is collinear with an axis defining the coordinate system in concern, so that lines in $\mathcal{M}_i^{\mathcal{A},\boldsymbol{p}}$ are not orthogonal to those in $\mathcal{M}_j^{\mathcal{A},\boldsymbol{p}}$ where $i \neq j$. To simplify the derivation of line equations in $\mathcal{M}_1^{\mathcal{A},\boldsymbol{p}}$, we introduce a base where lines in $\mathcal{M}_1^{\mathcal{A},\boldsymbol{p}}$ are parallel with the y-axis. Note that the same discussion can be applied to $\mathcal{M}_2^{\mathcal{A},\boldsymbol{p}}$ and $\mathcal{M}_3^{\mathcal{A},\boldsymbol{p}}$.

Let $\mathcal{A} = (a_x, a_y, a_z)^\top$ and $\boldsymbol{p} = (p_x, p_y, p_z)^\top$ in the standard orthonormal base B and the plane $\mathcal{P}$ with normal vector $\mathcal{A}$ that going through $\boldsymbol{p}$. Assuming lines in $\mathcal{M}_1^{\mathcal{A},\boldsymbol{p}}$ come from the intersection between $\mathcal{P}$ and the planes of the 3D half-grid that are parallel to yz-plane, we obtain the directional vector $\boldsymbol{v}_1$ of lines in $\mathcal{M}_1^{\mathcal{A},\boldsymbol{p}}$ as $\boldsymbol{v}_1 = \mathcal{A} \wedge \boldsymbol{e}_1$ where $\boldsymbol{e}_1 = (1,0,0)^\top$. We set $\boldsymbol{v}_2 = \frac{\boldsymbol{v}_1 \wedge \mathcal{A}}{\|\mathcal{A}\|}$, which is linearly independent of $\boldsymbol{v}_1$. Note that each of $\boldsymbol{v}_1$ and $\boldsymbol{v}_2$ is orthogonal with $\mathcal{A}$.

We introduce a new base B_1 in such a way that $\boldsymbol{v}_1$ and $\boldsymbol{v}_2$ respectively become $\boldsymbol{u}_1 = (1,0)^\top$ and $\boldsymbol{u}_2 = (0,1)^\top$ in $\mathcal{P}$. The transformation from B to B_1 is realized by

$$M_{BB_1} = \begin{pmatrix} 0 & \frac{a_z}{a_y^2 + a_z^2} & \frac{-a_y}{a_y^2 + a_z^2} \\ -\psi & \frac{\psi a_x a_y}{a_y^2 + a_z^2} & \frac{\psi a_x a_z}{a_y^2 + a_z^2} \end{pmatrix}, \tag{5}$$

where $\psi = \frac{1}{\sqrt{a_x^2 + a_y^2 + a_z^2}}$. We remark that $\mathcal{A}$ is transformed to $(0,0)^\top$ by M_{BB_1}; the rotation center in $\mathcal{P}$ thus becomes the origin of B_1.

Applying M_{BB_1} to the plane $x = k (k \in \mathbb{Z})$ induces a line in $\mathcal{M}_1^{\mathcal{A},\boldsymbol{p}}$ whose equation is

$$\psi(a_y^2 + a_z^2)y + k - \mathcal{A}.\boldsymbol{p}\psi^2 a_x = 0, \tag{6}$$

where $k \in \mathbb{Z}$.

Changing the roles between $\mathcal{M}_1^{\mathcal{A},\boldsymbol{p}}$ and $\mathcal{M}_2^{\mathcal{A},\boldsymbol{p}}$ ($\mathcal{M}_3^{\mathcal{A},\boldsymbol{p}}$, resp.) and between $\boldsymbol{e}_1$ and $\boldsymbol{e}_2 = (0,1,0)^\top$ ($\boldsymbol{e}_3 = (0,0,1)^\top$ resp.), we obtain the line equations for $\mathcal{M}_2^{\mathcal{A},\boldsymbol{p}}$ and $\mathcal{M}_3^{\mathcal{A},\boldsymbol{p}}$ with the bases B_i and the transformation matrices M_{BB_i} for $i = 2,3$:

$$\psi(a_x^2 + a_z^2)y + k - \mathcal{A}.\boldsymbol{p}\psi^2 a_y = 0, \tag{7}$$
$$\psi(a_x^2 + a_y^2)y + k - \mathcal{A}.\boldsymbol{p}\psi^2 a_z = 0, \tag{8}$$

where $k \in \mathbb{Z}$.

We remark that if $\mathcal{A}$ is collinear with one of the axes defining the coordinate system of the 3D space, M_{BB_i} degenerates: the rank of M_{BBi} becomes 1. In such cases, 3D rotations become identical with 2D rotations, which are not our concern here.

4.2   Quintuplet Integer Representation of Hinge Angles

A hinge angle in a given rotation plane is represented by a quintuplet of integers (p_x, p_y, p_z, i, k) given by $\alpha(p_x, p_y, p_z, i, k)$. Namely, we keep the coordinates of $\boldsymbol{p}$ and the information required for obtaining the coordinates of the arriving point $\boldsymbol{i}$ after the rotation of $\boldsymbol{p}$ by α. The first three integers p_x, p_y, p_z represent, in the old basis B, the coordinates of $\boldsymbol{p}$. The fourth integer i indicates the index number for the set $\mathcal{M}_i^{\mathcal{A},\boldsymbol{p}}, i = 1, 2, 3$, where the hinge angle α is defined. The last integer k represents the index number of the line in $\mathcal{M}_i^{\mathcal{A},\boldsymbol{p}}$.

From these five integers, we can obtain, in the basis B_i, the coordinates $(P_x, P_y)^\top$ and $(I_x, I_y)^\top$ of points $\boldsymbol{p}$ and $\boldsymbol{i}$ which define α as represented in Figure 5. The coordinates of $\boldsymbol{p}$ in B_i are obtained by applying M_{BB_i} to the coordinates of $\boldsymbol{p}$ in B. The coordinate I_y is obtained from one of (6), (7) or (8) depending on i. Since $\boldsymbol{i}$ belongs to the locus of the rotation of $\boldsymbol{p}$, we have $I_x^2 + I_y^2 = P_x^2 + P_y^2$ and deduce the value of I_x.

In general, I_x can take two values which define two points. To discriminate two different hinge angles corresponding to these two points by their integer quintuplets, we add the positive sign to the fourth integer for the greater I_x and the negative sign for another value of I_x. If $I_x = 0$, then the two points merge into one. This particular case where the locus of the rotation of $\boldsymbol{p}$ is tangent with the k-th line of $\mathcal{M}_i^{\mathcal{A},\boldsymbol{p}}$ does not define a hinge angle since there is no transition of convexel. Hereafter, the representation of hinge angles by integer quintuplets will be denoted by $\alpha(p_x, p_y, p_z, \pm i, k)$.

Note that according to Proposition 2 we know that any hinge angle cannot rotate a grid point to the intersection between two lines of a multi-grid. Therefore, two different integer quintuplets cannot represent the same hinge angle.

4.3   Rational Multi-grids

In Section 4.1, we obtained (6)-(8) for the lines in the multi-grid $\mathcal{M}^{\mathcal{A},\boldsymbol{p}}$. In general, parameters of these equations belong to $\mathbb{R}$. However in order to use only integers during computation, we need these parameters to belong to $\mathbb{Q}$.

If all elements of M_{BB_i} belong to $\mathbb{Q}$, then all the parameters of (6)-(8) become rational, so that $P_x, P_y, I_y \in \mathbb{Q}$. Even if $I_x \notin \mathbb{Q}$, $I_x^2 \in \mathbb{Q}$ because $I_x^2 = P_x^2 + P_y^2 - I_y^2$. Accordingly, computation can be realized as far as we use I_x^2. In order to obtain rational parameters in M_{BB_i} we set $\mathcal{A}$ to be a prime Pythagorean vector; a vector $\boldsymbol{v} = (i_1, i_2 \ldots, i_n)^\top, i_1, i_2, \ldots, i_n \in \mathbb{Z}$, is a Pythagorean vector if $\|\boldsymbol{v}\| = \lambda$ where $\lambda \in \mathbb{Z}$, and a Pythagorean vector $\boldsymbol{v}$ is prime if $\gcd(i_1, i_2, \ldots, i_n, \lambda) = 1$. Note that a rotation axis whose directional vector is such a prime Pythagorean vector is called a Pythagorean axis. This assumption ensures that $\mathcal{A}.\boldsymbol{p}$ becomes
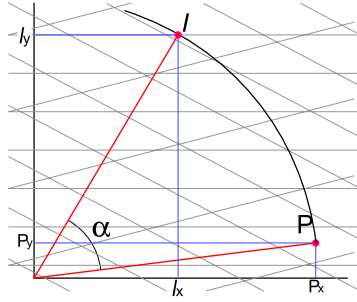
Fig. 5. A hinge angle α for a point $\boldsymbol{p}$ in a rational multi-grid

a rational value. We call a multi-grid defined from a Pythagorean axis a rational multi-grid.

In the following, we assume that all hinge angles are obtained in a rational multi-grid. In the next section we explain how rational multi-grids allow us to compare a pair of hinge angles using only integer computations in order to present a 3D discrete rotation algorithm.

5   3D Discrete Rotations around a Pythagorean Axis

In this section, we develop a 3D discrete rotation. This rotation is the extension to the 3D space of the 2D discrete rotation given in [12]. In order to estimate the complexity of the algorithm described in this section, we need to estimate the number of hinge angles existing for the image to rotate. In the case of 2D hinge angles, the upper bound of the number of different hinge angles for an image is given in [1,8]; we will use a similar method. Our algorithm, to be efficient, needs to compare a pair of hinge angles in constant time. Besides, in order to keep integer computation, we need that the comparison is done using only integers. Note that the hinge angle comparison in constant time is not indeed trivial due to our integer computation constraint. After giving the upper bound of the number of hinge angles for an image, we will show how to compare a pair of hinge angles in constant time and with integer computation, and then present a 3D discrete rotation algorithm for a given image.

In Section 5 we assume that $\mathcal{A}$ is given to be a prime Pythagorean vector.

5.1   Comparing Hinge Angles with Integer Computations

From the integer representation of hinge angles we can obtain the sine and cosine of a hinge angle $\alpha(p_x, p_y, p_z, \pm i, k)$. The following equations are derived from Figure 5:

$$\cos \alpha = \frac{P_x I_x + P_y I_y}{P_x^2 + P_y^2}, \tag{9}$$

$$\sin\alpha = \frac{P_x I_y - P_y I_x}{P_x^2 + P_y^2}, \tag{10}$$

where P_x, P_y, I_x, I_y are values obtained as described in Section 4.2.

Proposition 3. *Let α_1 and α_2 be two hinge angles defined for $\mathcal{A}$. Then it is possible to decide if $\alpha_1 > \alpha_2$ using only integer computations.*

Proof. *Let $\alpha_1 = \alpha(p_{1x}, p_{1y}, p_{1z}, \pm i_1, k_1)$ and $\alpha_2 = \alpha(p_{2x}, p_{2y}, p_{2z}, \pm i_2, k_2)$. Comparing α_1 and α_2 is equivalent to comparing their sines and cosines which are given in (9) and (10). First we compare the signs of both sine and cosine between α_1 and α_2. If the sines and cosines of both angles have different signs, then we can conclude whether $\alpha_1 > \alpha_2$ without other computation. Otherwise, without loss of generality, we can assume that both α_1 and α_2 belong to $[0, \frac{\pi}{2}]$, so that $\cos\alpha_i \geq 0$ and $\sin\alpha_i \geq 0$ for both $i = 1, 2$. As the method for comparing two sines is similar to the one for comparing two cosines, we will only show the later one.*

If α_1 is greater than α_2, $\cos\alpha_2 - \cos\alpha_1 > 0$. Thus we have, from (9),

$$(P_{1x}^2 + P_{1y}^2)(P_{2x}I_{2x} + P_{2y}I_{2y}) > (P_{2x}^2 + P_{2y}^2)(P_{1x}I_{1x} + P_{1y}I_{1y}). \tag{11}$$

For simplicity, let $A_1 = (P_{1x}^2 + P_{1y}^2)P_{2x}I_{2x}$, $B_1 = (P_{1x}^2 + P_{1y}^2)P_{2y}I_{2y}$, $A_2 = (P_{2x}^2 + P_{2y}^2)P_{1x}I_{1x}$ and $B_2 = (P_{2x}^2 + P_{2y}^2)P_{1y}I_{1y}$. Note that $A_1^2, B_1, A_2^2, B_2 \in \mathbb{Q}$. Now (11) is rewritten as

$$A_1 + B_1 > A_2 + B_2. \tag{12}$$

Squaring both sides of (12) since they are not negative, and moving rational values to the left-hand side and irrational values to the right-hand side, we obtain

$$A_1^2 + B_1^2 - A_2^2 - B_2^2 > 2A_2B_2 - 2A_1B_1. \tag{13}$$

If the left-hand side and the right-hand side of (13) do not have the same sign, then we can conclude whether $\alpha_1 > \alpha_2$ or $\alpha_2 > \alpha_1$. We can check the sign of both sides of (13) with integer computations since the left-hand side contains only rational numbers and the sign of the right side is the same as $A_2^2B_2^2 - A_1^2B_1^2$ which also contains only rational numbers. If signs of both sides are the same, assuming that they are positives, we square both sides of (13) to obtain

$$(A_1^2 + B_1^2 - A_2^2 - B_2^2)^2 - 4A_1^2B_1^2 - 4A_2^2B_2^2 > -8A_1B_1A_2B_2. \tag{14}$$

If the sign of the left-hand side of (14) is positive, we can deduce that $\alpha_2 > \alpha_1$. Otherwise, taking the square of each side gives us

$$\left[(A_1^2 + B_1^2 - A_2^2 - B_2^2)^2 - 4A_1^2B_1^2 - 4A_2^2B_2^2\right]^2 < 64A_1^2B_1^2A_2^2B_2^2. \tag{15}$$

We note that we can easily verify whether (15) is satisfied with integer computation alone. If (15) is true, $\alpha_1 < \alpha_2$; otherwise $\alpha_2 < \alpha_1$. The same logic can be applied to the case where the signs of the both sides of (13) are negative. $\square$

Thanks to Proposition 2, a hinge angle cannot have two quintuplet integer representations. Thus we can conclude that the comparison of a pair of hinge angles α_1, α_2 is always possible with integer computation if they have different quintuplets.

Note that the comparison of a pair of hinge angles is done in constant time because in the worst case, we only have to check (13),(14) and (15). It seems obvious that the comparison is done in constant time. However, keeping integer computation may increase the number of necessary comparisons. From Proposition 3, we now have a guarantee of a constant number for each comparison.

In the 2D case, is it known that the comparison between a hinge angle and a Pythagorean angle can be also done using only integers during its computation and in constant time. An angle is a Pythagorean angle if its sine and cosine belong to $\mathbb{Q}$ [8]. In the 3D case, the similar proposition is still valid. This proposition is required for our algorithm of 3D discrete rotation.

Proposition 4. *Let α be a hinge angle and θ be a Pythagorean angle defined for $\mathcal{A}$. Then it is possible to decide if $\alpha > \theta$ in constant time with integer computations.*

The proof of Proposition 4 is similar to the proof on comparison for a hinge angle and a Pythagorean angle in the plane [12]. Due to the page limitation, we skip the proof.

5.2   Upper Bound of the Number of 3D Hinge Angles

In the 2D case, the upper bound of the number of hinge angles for a given image of size $m \times m$ is known to be $O(m^3)$ [8]. This is obtained by computing the bound for the furthest point from the origin in the image and multiplying this bound by the number of points in the image. To compute the number of hinge angles in the 3D case, we will use a similar method.

In the 3D case, we assume that an image of size $m \times m \times m$ is given. The number of hinge angles for a given point $\boldsymbol{p}$ depends on the distance between $\boldsymbol{p}$ and the axis of rotation $\boldsymbol{A}$. Therefore, we define the distance function $d(\boldsymbol{p})$ that is the Euclidean distance between $\boldsymbol{A}$ and $\boldsymbol{p}$. Then, the rotation of $\boldsymbol{p}$ around $\boldsymbol{A}$ intersects at most $3\lfloor d(\boldsymbol{p}) \rfloor$ planes of the half-grid and defines at most $6\lfloor d(\boldsymbol{p}) \rfloor$ different hinge angles. Because $d(\boldsymbol{p}) \leq \sqrt{3}m$, the upper bound of the number of hinge angles for any point in the image is $6\sqrt{3}m$. Accordingly, we can conclude that the upper bound of the number of hinge angles for a given image of size $m \times m \times m$ is $6\sqrt{3}m^4$; thus $O(m^4)$.

5.3   3D Discrete Rotations Induced by Hinge Angles

In this section, we explain how to design a discrete rotation of a 3D digital image using hinge angles for a given Pythagorean axis of rotation. This method is the 3D extension of the 2D discrete rotation described in [12]. As input of such discrete rotation, we have a digital image $\mathcal{I}$ of size $m \times m \times m$, a vector $\mathcal{A}$, supposed to

---

Algorithm 1. Rotation of a 3D image around an integer-axis whose direction is $\mathcal{A}$ by a Pythagorean angle θ

Input: An image $\mathcal{I}$, a vector $\mathcal{A}$, a Pythagorean angle θ
Output: A rotated image $\mathcal{I}'$

 1: L<- An empty list;
 2: **for all** Points $\boldsymbol{p}$ in $\mathcal{I}$ **do**
 3:     Compute the three generic equations (6)-(8) of $\mathcal{M}_1^{\mathcal{A},\boldsymbol{p}}, \mathcal{M}_2^{\mathcal{A},\boldsymbol{p}}, \mathcal{M}_3^{\mathcal{A},\boldsymbol{p}}$;
 4:     **for all** k-th lines in $\mathcal{M}_i^{\mathcal{A},\boldsymbol{p}}, i = 1, 2, 3$ **do**
 5:         Compute all hinge angles corresponding to $\boldsymbol{p}$ and the k-th line
 6:         of $\mathcal{M}_i^{\mathcal{A},\boldsymbol{p}}$ and add $\alpha(p_x, p_y, p_z, \pm i, k)$ to the list L;
 7:     **end for**
 8:     Sort hinge angles corresponding to $\boldsymbol{p}$;
 9:     Search in L the greatest hinge angle α which is smaller than θ;
10:     Copy the image value from $\boldsymbol{p}$ to the rotated point with α in $\mathcal{I}'$
11: **end for**
12: **return** $\mathcal{I}'$;

---

be a prime Pythagorean vector, and an angle θ supposed to be Pythagorean [8]. The assumption that the rotation axis is a Pythagorean axis and the angle is a Pythagorean angle does not restrict the field of possible rotations because in [11] it is proved that the Pythagorean vectors are dense in the 3D space and in [5] it is proved that any angle can be approximated with a small difference $\epsilon > 0$ by a Pythagorean angle. The output is a rotated digital image $\mathcal{I}'$.

The rotation algorithm is described in Algorithm 1. For each point $\boldsymbol{p} = (p_x, p_y, p_z)^\top$ in the image, the algorithm computes the corresponding multi-grid $\mathcal{M}^{\mathcal{A},\boldsymbol{p}}$ and search for each line k-th in $\mathcal{M}_i^{\mathcal{A},\boldsymbol{p}}, i = 1, 2, 3$, a pair of hinge angles $\alpha(p_x, p_y, p_z, \pm i, k)$. Then we stock and sort all hinge angles corresponding to $\boldsymbol{p}$ using Proposition 3. The algorithm searches in the sorted list the greatest hinge angle α which is smaller than θ using Proposition 4. This operation can be done using only integer computations thanks to our assumption that θ is a Pythagorean angle. Finally the new point after the rotation of $\boldsymbol{p}$ by α is generated in $\mathcal{I}'$.

The time complexity of this algorithm is $\mathrm{O}(m^4 \log m)$. The computation and the sorting of all hinge angles for each point is done in $\mathrm{O}(m \log m)$ operations because the comparison between two hinge angles is done in constant time according to Proposition 3. Searching the largest hinge angle α smaller than θ is done in $\mathrm{O}(m)$ operations because the comparison between a hinge angle and a Pythagorean angle can be performed in constant time according to Proposition 4. Therefore, the time complexity of this algorithm is $\mathrm{O}(m^4 \log m)$ because we repeat m^3 times the previous operations.

Note that Algorithm 1 describes a classic rotation. In [8], the author describes a 2D incremental rotation that allows obtaining all possible configurations of 2D discrete rotations for a given image. Hinge angles on rotation planes also allow us to design a 3D incremental discrete rotation.

6   Conclusion

In this paper, we extended the notion of hinge angles, introduced for 2D discrete rotation in [8,12] to the 3D. Extension of hinge angles from the 2D to 3D space involves many problems because most of properties of 2D hinge angles are not valid for 3D hinge angles. In order to regard hinge angles in the 3D space similarly to the 2D ones, we introduced the notion of a multi-grid that is the intersection of the 3D half-grid and a rotation plane. By redefining the hinge angles on the rotation plane, which are the extension of hinge angles for the rotation in 2D, we showed a subgroup of the multi-grids where all parameters are rational, called rational multi-grids. This subgroup allows us to compare two hinge angles on rotation planes in constant time by using integer computations. It also allows us to design a 3D discrete rotation.

In [9], the authors studied particular configurations induced by 2D discrete rotations, which provided their periodicity and neighborhood properties. Our future work will be, by using multi-grids and 3D hinge angles, to extend their work to 3D discrete rotations.

References

1. Amir, A., Butman, A., Crochemore, M., Landau, G.M., Schaps, M.: Two-dimensional pattern matching with rotations. Theor. Comput. Sci. 314(1-2), 173–187 (2004)
2. Andres, E.: Cercles discrets et rotations discrètes. PhD thesis, Université Louis Pasteur, Strasbourg, France (1992)
3. Andres, E.: The quasi-shear rotation. In: Miguet, S., Ubéda, S., Montanvert, A. (eds.) DGCI 1996. LNCS, vol. 1176, pp. 307–314. Springer, Heidelberg (1996)
4. Andres, E., Sibata, C., Acharya, R., Shin, K.: New methods in oblique slice generation. In: SPIE Medical Imaging 1996. SPIE, vol. 2707, pp. 580–589 (1996)
5. Anglin, W.S.: Using pythagorean triangles to approximate angles. American Mathematical Monthly 95(6), 540–541 (1988)
6. Chen, B., Kaufman, A.: 3d volume rotation using shear transformations. Graphical Models 62, 308–322 (2000)
7. Hartley, R., Kahl, F.: Global optimization through rotation space search. International Journal of Computer Vision 82(1), 64–79 (2009)
8. Nouvel, B.: Rotations discrètes et automates cellulaires. PhD thesis, Ecole Normale Supèrieure de Lyon, France (2006)
9. Nouvel, B., Rémila, E.: Configurations induced by discrete rotations: periodicity and quasi-periodicity properties. Discrete Applied Mathematics 147(2-3), 325–343 (2005)
10. Schmidt, J., Niemann, H.: Using quaternions for parametrizing 3-d rotations in unconstrained nonlinear optimization. In: VMV 2001: Proceedings of the Vision Modeling and Visualization Conference, Aka GmbH, pp. 399–406 (2001)
11. Thibault, Y., et al.: Density of pythagorean n-tuples (in preparation)
12. Thibault, Y., Kenmochi, Y., Sugimoto, A.: Computing upper and lower bounds of rotation angles from digital images. Pattern Recognition 42(8), 1708–1717 (2009)
13. Toffoli, T., Quick, J.: Three-dimensional rotations by three shears. CVGIP: Graphical Model and Image Processing 59(2), 89–95 (1997)
14. Voss, K.: Discrete Images, Objects and Functions in Z^n. Springer, Heidelberg (1993)